Journal of Materials Chemistry C

ROYAL SOCIETY OF CHEMISTRY

PAPER

View Article Online
View Journal | View Issue

Cite this: J. Mater. Chem. C, 2025, 13, 19444

Impact of dopant geometry on memristive properties of oriented layers of conjugated macromolecular nanowires

Wojciech Wieczorek, [ab] Tomasz Kuciel,[c] Tomasz Mazur,[b] Krystian Sokołowski, [b] Konrad Szaciłowski [b] and Michał Szuwarzyński *[b]

Received 23rd April 2025,
Accepted 7th August 2025

DOI: 10.1039/d5tc01634g

rsc.li/materials-c

Memristive materials are of great interest due to their potential in modern electronics and computing technologies. While most studies focus on inorganic systems, organic and polymer-based alternatives are also emerging. This work presents surface-grafted polymer brushes with conjugated polyacetylene chains as an efficient memristive system and explores their tunability through doping with inorganic salts. The brushes were synthesized in a two-step process, starting with polymethacrylate brushes obtained *via* surface-initiated photoiniferter-mediated radical polymerization. Characterization using AFM, XPS, and FTIR confirmed the presence of tetrahedral $[FeCl_4]^-$ and linear $[CuCl_2]^-$ counterions incorporated into the conjugated chains. The doping process, performed for 10 and 60 minutes, shows pinched hysteresis loop. The influence of doping and dopant geometry on electrical, memristive, structural properties, and film thickness was analyzed. Additionally, experimental findings were supported by DFT modeling, providing deeper insights into the behavior of the system.

1. Introduction

Advances in information technology, particularly in artificial intelligence, are driving an ever-growing demand for computational power and data storage. The neuromorphic design of devices offers a promising route to overcome some of the limitations of traditional systems, especially those related to energy consumption and data transfer issues.[1,2] In contrast to silicon semiconductors[3] and von Neumann architecture separating computational and memory units,[4] human brains are composed of complex neural networks communicating through nanoscale gaps called synapses facilitating learning.[5] Some of their properties can be observed in synthetic systems known as memristors. Memristors, known also as memory resistors, are a class of passive two-terminal electronic components that exhibit a unique relationship between electrical charge and magnetic flux.[6] First theorized in 1971 by Chua[7] and later demonstrated in a practical form by researchers at Hewlett-Packard Labs in 2008,[8] memristors represent the fourth fundamental circuit elements, alongside resistors, capacitors, and inductors. The defining characteristic of memristors is their ability to retain memory of their electrical resistance state, which depends on the history of the voltage applied to them and the current passed through them.[9] Unlike traditional resistors, for which resistance remains fixed, a memristor's resistance can change depending on the magnitude and direction of the applied voltage, and the memristor itself can hold this resistance state even after the current flow is turned off. This property makes them particularly appealing for non-volatile memory applications, where information storage remains intact without the need for continuous power. In contrast to contemporary storage systems, a resistance change between the ON and OFF states is gradual and depends on the history of the applied current, mimicking synaptic plasticity[10] and potentially allowing both data storage and computing functionality in the same physical entity. The first physical memristive systems were based on titanium oxide.[8] Since then, systems based on ferroelectrics,[11] perovskites,[12] multiferroics,[13] spintronic systems,[14] biomolecules[15] and small organic molecules[16] were explored. Moreover, there were also few attempts based on polymers, mainly on conjugated polymer chains[17] or non-conjugated polymers with pendent chromophores[18] which, combined with the properties of the polymers themselves, brings several key advantages. They are lightweight, elastic, do not depend on potentially toxic heavy metals, and can be relatively easily prepared in various shapes or forms, including thin layers, which can be used as

[a] AGH University of Krakow, Faculty of Materials Science and Ceramics, Mickiewicza 30, 30-059, Krakow, Poland
[b] AGH University of Krakow, Academic Centre for Materials and Nanotechnology, Mickiewicza 30, 30-059, Krakow, Poland. E-mail: szuwarzy@agh.edu.pl
[c] Jagiellonian University, Faculty of Chemistry, Gronostajowa 2, 30-387, Krakow, Poland

two-dimensional standalone memristive devices[19] or as part of a hybrid system.[20]

Polyacetylene is the simplest possible conjugated polymer and the first to be discovered.[21] It is a semiconductor,[22] but it exhibits metallic conductivity after doping.[23] Polyacetylenes can be doped with protic acids,[24] strong reductors[25] or most commonly by oxidation with halogens or Lewis acids. Oxidation of chains introduces positive charge carriers in their structure compensated by anions produced by the dopants reduction.[26] The dopant concentration is usually much higher than in typical silicon semiconductors,[27] so much so that heavily doped systems may exhibit some properties of dopants themselves.[28] While the use of polyacetylene is hampered by its fibrous, unstable, and insoluble nature,[29] a wide range of conjugated polymers have since been discovered[30] forming a backbone of polymer light-emitting diodes,[31] organic field effect transistors[32] and organic photovoltaics.[33] Memristive switching in conjugated polymers usually follows acceptor–donor charge transfer or reversible redox mechanism.[34] Polyacetylene, in addition to the bulk form, can be obtained as a system grafted from the surface, taking the conformation of polymer brushes.[35] It has been shown that such systems remain stable over time and retain their conductive properties much longer than their free analogues.[36] Surface-grafted polymer brushes are macromolecular thin layers, made of polymer chains with one end tethered to a surface densely enough so that interactions between them result in maintaining an extended conformation.[37] Brushes provide a highly ordered, anisotropic environment preventing aggregation which can hamper the reproducibility of system performance[38,39] making them promising candidates for nanoelectronics, including memristive systems. In this work we present surface-grafted brushes with conjugated polyacetylene chains prepared in a two-step scheme, beginning with obtaining polymethacrylate brushes with reactive side groups using surface-initiated reversible deactivation radical polymerization reactions[40] which are more convenient and allow for greater control of density and length of grafted structures. The side groups later serve as macromonomers for template polymerization resulting in a ladder-like structure of polyacetylene. Poly(3-trimethylsiliylpropagyl methacrylate) (TPM) brushes were obtained by surface-initiated photoiniferter-mediated radical polymerization. Its side groups contain protected terminal triple bonds useful for various click reactions[41,42] which can also be polymerized leading to the double-stranded polymer brushes composed of the main chain providing a durable backbone for a parallel polyacetylene chain.[33,34] When such systems are doped with nonvolatile, stable dopants[43] it is expected that the doping redox process may be reversible by electric flux. Memristive properties of such systems were investigated concerning the shape of *I–V* loop. Both were determined by solid-state variation cyclic voltammetry with a hanging mercury electrode, while stability and the nature of doping were investigated using atomic force microscopy and various spectroscopic techniques.

2. Results and discussion

To address the characterization of doped systems, the efficiency of obtaining native poly(TPM) brushes grafted from an ITO substrate must first be determined. The dependence of the thickness of the obtained polymer layer on the PIMP photopolymerization time is a well-known behavior,[38] however, a series of poly(TPM) substrates was made after 2, 4, 8 and 12 h of 50 W UV lamp exposure with a wavelength of 275 nm and a constant sample-lamp distance. As expected, the thickness of the poly(TPM) brushes was getting higher: after 2 h was 23.9 ± 0.5 nm, after 4 h – 28.8 ± 0.9 nm, after 8 h – 35.9 ± 0.3 nm and after 12 h – 50.1 ± 0.8 nm (see Fig. S4). Comparing the thickness of the obtained layers to its quality and homogeneity, 8 h was selected as the most satisfactory time for all further experiments. To bring the brush system to conductive and memristive properties, first it must be created a path of conjugated –C=C– bonds in the poly(TPM) matrix. This is possible because of the self-templating polymerization reaction, which involves deprotected triple bonds in the side groups of polymer brushes. Each step of this process: native brushes, brushes after cleavage of protecting trimethylsiliyl (TMS) groups and brushes after self-template polymerization were characterized by atomic force microscopy, FTIR spectroscopy and XPS (see Fig. 1). AFM topography images show a homogeneous surface structure, which becomes smooth after deprotection and removal of the TMS groups from the brush systems. Surface roughness (RMS, R_q) decreases from 5.45 ± 0.13 nm for native poly(TPM) brushes to 3.66 ± 0.11 nm, which is caused by the collapse and tighter packing of the modified side groups in the dry brush system. Carrying out self-template polymerization results in the formation of conjugated double bonds that stiffen the entire structure. The conformation of the system becomes more straightened, resulting in an increase in the surface roughness to a value of 5.28 ± 0.15 nm. The FTIR spectra clearly confirms the effectiveness of the performed cleavage of protective groups and self-template polymerization reactions. The self-template polymerization of the side acetylene groups was conducted using a rhodium-based catalyst (Rh-cat, bicyclo[2.2.1]hepta-2,5-diene-rhodium(I) chloride dimer) and the results of this reaction are visible by the decrease in the characteristic band at 2100–2200 cm^{-1} assigned to –C≡C– vibration accompanied by the appearance of the strong band at 1540 cm^{-1} characteristic of –C=C– vibrations in the created polyacetylene conjugated chain.[44] Moreover, XPS spectra confirm the effectiveness of the performed reaction. First, the quantitative composition of the layers was revealed by acquiring full-range scans depicted in Fig. 1. As expected, the acquired survey scans revealed signals from the atoms made the brushes and some traces from the ITO substrate, probably due to discontinuities of the prepared layers. Particularly important are the changes for silicon that concern the reduction of its concentration in native brushes from 7.2 to 1.4 at% after the second step of synthesis, as well as the changes in carbon atoms content related to the increase in their concentration (from 72.4 to 78.0 at%) in the layer subjected to self-template polymerization. To confirm the existence of a given reaction in the synthesis pathway, the chemical environment of silicon, oxygen and carbon atoms was analyzed by recording and fitting high resolution spectra in the Si 2p,

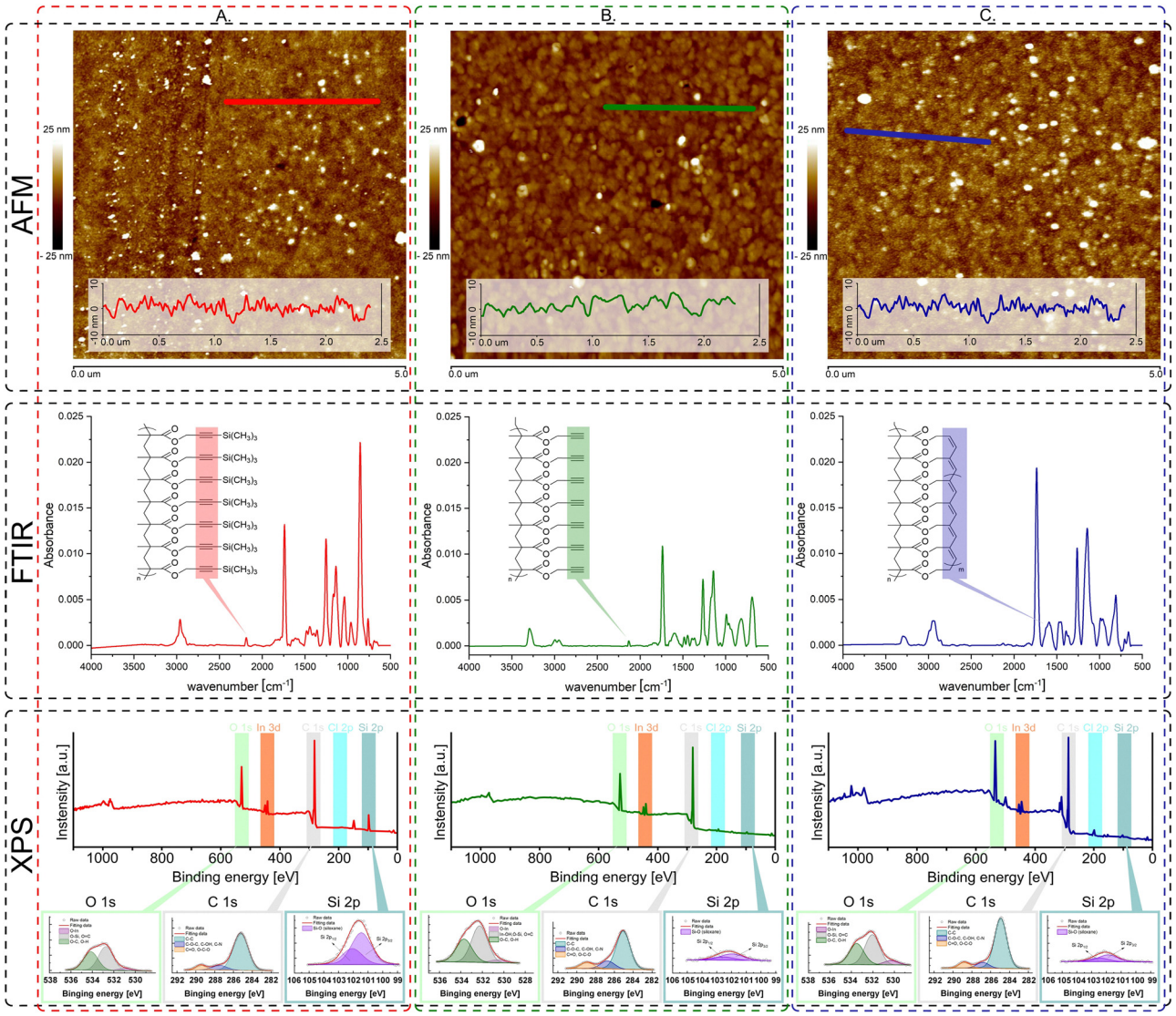

Fig. 1 AFM, FTIR and XPS characteristic of native poly(TPM) brushes (A), poly(TPM) brushes after cleavage of protecting TMS groups (B) and poly(TPM) brushes after self-template polymerization (C).

C 1s, and O 1s regions, as shown in Fig. 1. The Si 2p spectra for all samples show one doublet structure (doublet separation $p_{3/2}$–$p_{1/2}$ equals 0.61) with main $2p_{3/2}$ line at 101.9 eV which indicates Si–O–C species like in photoiniferter and/or TMS.[45,46] The achieved reduction of the Si 2p doublet intensity in the second step of the synthesis proves the successful cleavage of TMS groups, leaving small signals from the photoiniferter. The C 1s spectra of all layers were fitted with three components with the first line at 285.0 eV from C–C bonds, the second line at 286.8 eV which indicates presence of C–O bonds, and the last line at 288.9 eV assigned to either C═O and/or O–C–O groups.[47] The intensity of oxygen-containing groups remains at a similar level during synthesis. The more important changes in the C 1s spectrum are concerned with the main line at 285.0 eV and appear during the third stage, where one can observe a reduction in the line thickness and an increase in intensity, which is a typical behavior for sp^2 carbon and proves the formation of conjugated –C═C– bonds in the poly(TPM) matrix. The O 1s spectra of samples also were fitted with three components. The first line is found at 529.7 eV which indicates the presence of metal oxides (O–In, O–Sn), the second line at 531.4 eV indicates metal hydroxide ($In(OH)_3$) and O═C bonds, and the last line at 532.4 eV originates either from O–Si and/or O–C and/or –OH type species.[48,49]

Having confirmed the effectiveness and repeatability of obtaining polymer brushes with a conjugated –C═C– bond, the next step was to dope the obtained structure ith $FeCl_3$ and $CuCl_2$ salts. Both inorganic, low-molar-mass compounds, although similar in chemical structure (chlorides, d-block metal cations), have completely different spatial conformations, which seem to be key to tuning the conductive and memristive properties. The formed $[FeCl_4]^-$ counterions, built into the conjugated chain in the poly(TPM) brushes, had a tetrahedral structure, while $[CuCl_2]^-$ had a linear structure.

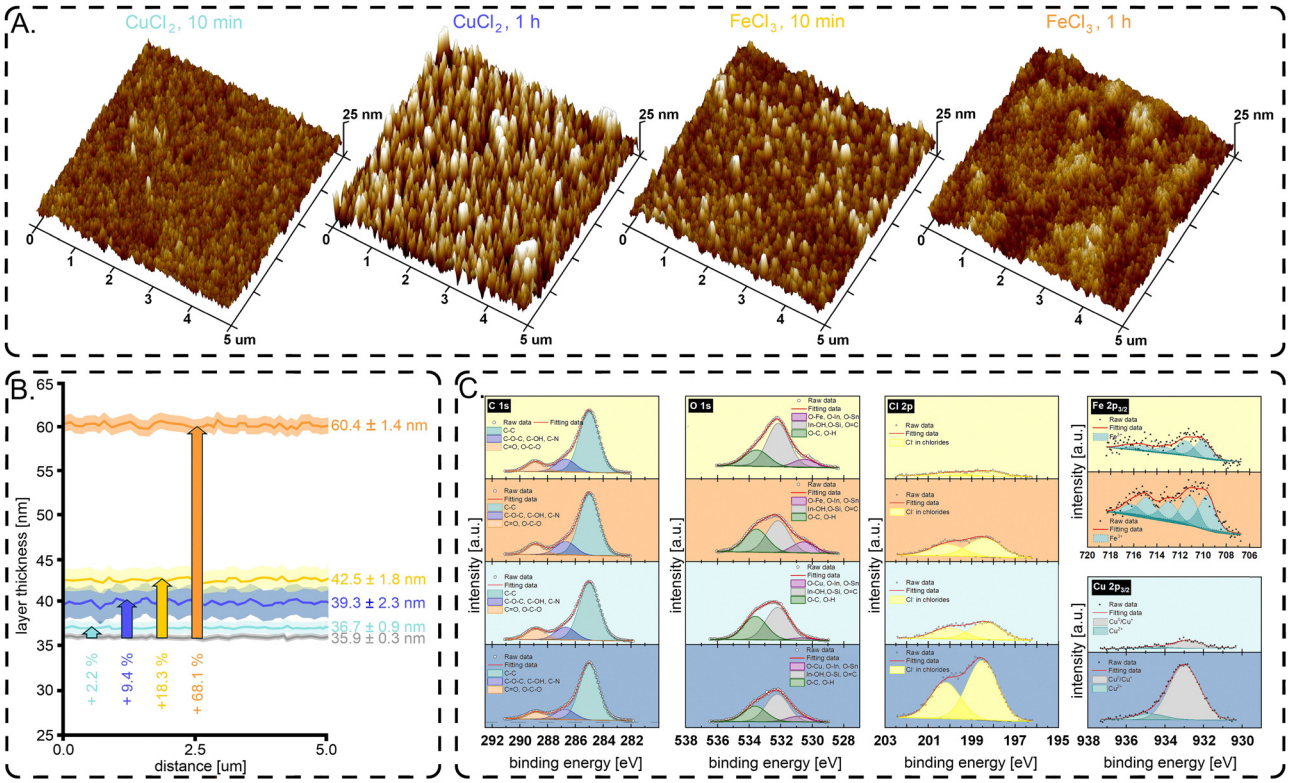

Fig. 2 (A) AFM 3D topography renders of poly(TPM) brushes after self-template polymerization doped with $FeCl_3$ and $CuCl_2$ after 10 min and 60 min of doping reaction, (B) average thickness of all doped poly(TPM) coating with corresponding percentage changes compared to native poly(TPM) brushes (gray), (C) XPS C 1s, O 1s, Cl 2p, Fe $2p_{3/2}$ and Cu $2p_{3/2}$ spectra for doped poly(TPM) brushes. In all images the relevant systems are color coded: $FeCl_3$ after 10 min: yellow, $FeCl_3$ after 1 h: orange, $CuCl_2$ after 10 min: bright blue, $CuCl_2$ after 1 h: dark blue.

These data, although known from the literature,[50,51] were confirmed using the XPS technique (Fig. 2C and the SI Paragraph S4), the spectra of which clearly suggest the presence of Fe^{3+} ions in the spectrum of poly(TPM) doped with $FeCl_3$ and Cu^{+} ions (and to a Cu^{2+} occurring in smaller quantities) in $CuCl_2$ doped systems. The amount of both iron and copper ions in the systems varies and increases with increasing doping time. While the roughness (RMS, R_q) of the measured surface for each of the tested systems does not show any significant trends (Fig. 2A): 4.2 ± 0.6 nm for $CuCl_2$ (10 min), 8.3 ± 1.4 nm for $CuCl_2$ (1 h), 5.6 ± 1.1 nm for $FeCl_3$ (10 min), 5.2 ± 0.9 nm for $FeCl_3$ (1 h), some interesting behaviours can be noticed when measuring the cross-sections of the layers obtained after doping. What is consistent with simulated DFT data (molecular volume for $[FeCl_4]^-$ counterion is 162.87 Å^3, for $[CuCl_2]^-$ is 87.90 Å^3, see SI Paragraph S5) the layer growth, compared to native poly(TPM) (35.9 ± 0.3 nm), was greater for $[FeCl_4]^-$ counterions, due to its large spatial conformation. $[FeCl_4]^-$ counterions straighten the polymer chains more, lifting the entire brush structure upwards. The thickness of brushes after 10 min of $FeCl_3$ doping time was 42.5 ± 1.8 nm, which is an increase of +18%, while the analogous doping of $CuCl_2$ increased the layer by only 2.2% to an average value of 36.7 ± 0.9 nm. Moreover, longer doping time (1 h), as we know from the XPS spectra, resulted in placing a larger amount of counterions in the polymer brush matrix, which increased layer thickness to the value of 39.3 ± 2.3 nm (+9.4%) for $CuCl_2$ and to 60.4 ± 1.4 nm (+68.1%) for $FeCl_3$ (Fig. 2B).

Having confirmed that the obtained structures were modified in the desired way, we carried out the electrical characterization of all poly(TPM) systems. All of the samples were measured for their *I*–*V* characteristic, as shown in Fig. 3a – within −500 mV and +500 mV limits. In order to analyze other voltage ranges, see Fig. S6. The undoped sample exhibited a diode-like behavior with forward-to-backward current ratio of 2.82. This values is not spectacular, but clearly indicated the partial rectifying character of the junction.[52] The forward current shows a purely exponential dependence on the applied bias, thus indicating the character of thermionic emission, typical for the Schottky barriers (Fig. 3d–h and eqn (1)):[53]

$$I = I_0\left(\exp\left(\frac{eU}{k_B T}\right) - 1\right) \quad (1)$$

where I_0 is the saturation current, e in an elemental charge, U is applied bias, k_B is the Boltzmann constant and T is the temperature in the absolute scale. Upon doping for 10 minutes with either $CuCl_2$ or $FeCl_3$ a this typical Schottky junction characteristics evolves toward memristor-like hysteresis loop. With prolonged doping (1 h) the behavior shifted back to a reduced hysteresis and partial restoration of the diode-like characteristic. Conductivity increased significantly after 10 min of doping but decreased with further doping time,

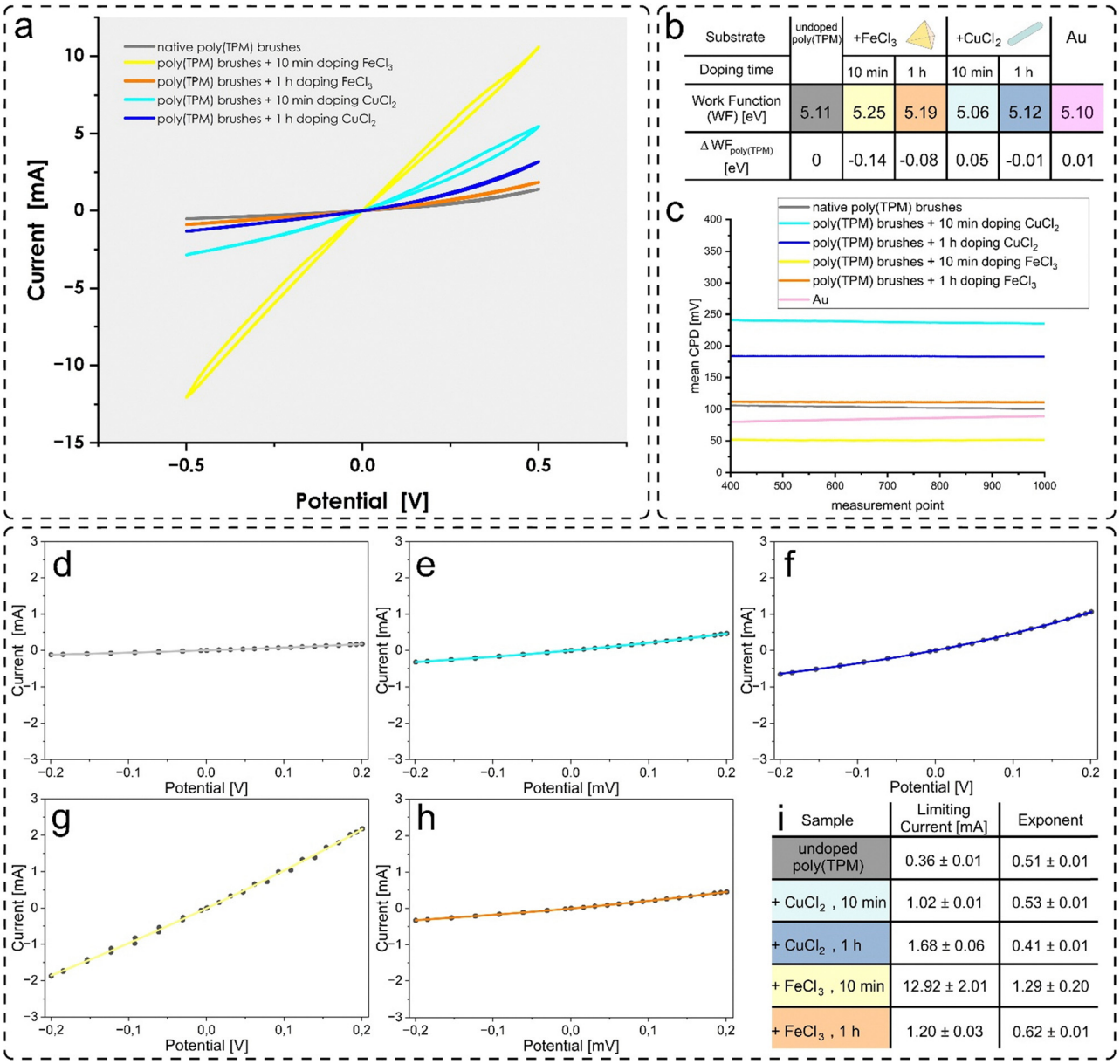

Fig. 3 (a) Averaged ten *I*–*V* scans, the responses are presented for different poly(TPM)-based samples: undoped (gray line), $FeCl_3$ after 10 min: yellow, $FeCl_3$ after 1 h: orange, $CuCl_2$ after 10 min: bright blue, $CuCl_2$ after 1 h: dark blue; (b), WF of various types of poly(TPM)-based samples with ΔWF – differences from undoped poly(TPM) sample; (c) changes in the mean values of CPD for different poly(TPM) doped and undoped samples with additional signal from gold plate standard. CPD was registered for 1000 point per sample. Measurements shown are for ambient conditions and for samples put in faradaic cage, current–voltage plots of the poly(TPM) brushes fitted with exponential model: native poly(TPM) (d), $CuCl_2$ after 10 min (e), $CuCl_2$ after 1 h (f), $FeCl_3$ after 10 min (g) and $FeCl_3$ after 1 h (h); (i) Fitting parameters from eqn (1).

although it remained higher than for the undoped sample. Fitting yields the limiting current values for all layers, the lowest for undoped polymer (0.36 mA) and the highest for $FeCl_3$ one (after 10 minutes doping, 12.92 mA). All fitting data are collated in Fig. 3i. This behavior reflects changes in the band structure induced by doping, and diminishing the original diode characteristic. Comparative analysis of the positive and negative currents revealed that while the samples retained dominant Ohmic contact properties, the hysteresis span increased significantly, indicating influence from a variety of conduction, modification and switching mechanisms. These include Ohmic conductivity, interfacial junction modifications for Schottky type of diodes, resistive switching driven by structural changes in the polymer brushes but also the inertia of doped complex compounds movement in an external potential. All of the latter, highlight the vast interplay of mechanisms contributing to the overall resistive switching and in consequence memristive behavior. Registered changes demonstrate how doping time influences electronic and interfacial properties. Control factors over device performance will be similar to redox-based valence change memories (VCM).[54]

One possible explanation for this behavior is the modification of the functional layer work function (WF) resulting from

changes in the structural composition of the layer, which subsequently affects the interfacial properties. The shapes and hysteresis span suggest that the switching is primarily an interfacial phenomenon, likely occurring at the poly(TPM)/Hg junction. Ambient KP measurements support this hypothesis for both types of dopants. Fig. 3b presents a table with the WF values, alongside the gold electrode WF, which is standardized by the literature (5.10 eV). Upon doping (10 min), the WF of poly(TPM) samples initially deviated from that of the undoped sample but returned closer to the undoped WF after prolonged doping (1 h). Considering the interfacial switching mechanism, these changes in the WF are expected to influence both the hysteresis range and the mean conductivity ranges, as potentially reflected in the *I–V* characteristics shown in Fig. 3a. The *I–V* response exhibits a distinct memristive behavior in samples doped for only 10 minutes; however, this characteristic diminishes with prolonged doping. The experimental stability of the mean CPD values is shown in Fig. 3c, provides additional insight into the consistency of these measurements. KPFM measurements were used to determine the work function (WF) of devices fabricated with different materials. The results revealed that poly(TPM) samples subjected to prolonged doping with $CuCl_2$ or $FeCl_3$ exhibited WF values comparable to the undoped poly(TPM) sample. To achieve this, the WF of the measurement tip was first calibrated using a gold standard, known to have a WF of 5.10 eV. Subsequently, the contact potential difference (CPD) of the sample surface was measured and added to the tip's WF, resulting in the calculated WF for the material.

The nonlinearity of the *I–V* characteristic for undoped (Fig. 3d) and doped (Fig. 3e–h) polymer films indicates typical thermionic emission characteristics of the Schottky barrier. Thus, it implies that the barrier at the mercury/polymer interface plays a crucial role in transport phenomena across thin polymeric films. It is fully justified because conjugated chains (both undoped and fully doped) should contribute to hopping and metallic-type conductivity, respectively. Both should present linear (or almost linear) current–voltage characteristics. Interestingly, moderate (10 min) doping, regardless of the nature of the dopant, results in the largest change in the work function value (decrease for $FeCl_3$ and increase for $CuCl_2$). Furthermore, these moderate doping levels (especially with iron salt) result in an opening of a hysteresis loop. The increased conductivity and exponential-to-linear current–voltage dependence transition with concomitant opening of the hysteresis loop indicate complete rearrangement of the electronic structure of the polymer film. It can be attributed to an optimal doping level corresponding to metallic-like conductivity of the layer, and a contribution on interfacial redox process responsible for hysteresis.[55,56] The clockwise direction of hysteresis in the 1st quadrant (*e.g.* transition for low-resistive to high-resistive state upon increased bias voltage) suggests contribution of polymer-based redox processes in resistive switching. The moderately doped polymer is more conductive than the undoped polymer and in addition, subsequent oxidation at positive potential values results in decreased conductivity. The differences in backward and forward electron transfer rates across the mercury/polymer interface are thus the immediate reason of the observed hysteresis.

3. Conclusions

In this work, we presented an ordered surface-grafted system of polymethacrylate brushes (poly(TPM)) modified *via* self-template polymerization, forming conjugated polyacetylene –C═C– bonds. Brushes with propagyl side groups were obtained by using controlled surface-initiated photoiniferter-mediated radical polymerization (SI-PIMP) and modified with a rhodium(I) chloride compound. Such reaction leads to the fabrication of semiconductor conduction paths through the formed conjugated –C═C– bonds, but it is not free from heterogeneity, mutual cross-linking, or the formation of discontinuities in the structure. However, these potentially unwanted properties turned out to be crucial for our systems to have memristive properties. After material characterization of the obtained layers (AFM, FTIR, XPS), we showed that native poly(TPM) brushes have a small hysteresis loop on the *I–V* curve. To improve memristive properties, we doped the poly(TPM) system with $CuCl_2$ and $FeCl_3$ salts for 10 and 60 min. The AFM cross-sectional images and the XPS spectra clearly showed different amounts of incorporated dopants in the form of $[CuCl_2]^-$ and $[FeCl_4]^-$ counterions. Using DFT modeling, we determined that the $[CuCl_2]^-$ structure is linear with a molecular volume of 87.90 and the $[FeCl_4]^-$ structure is tetragonal with a molecular volume of 162.87. While maintaining a constant amount of substituted salt (from XPS: 0.5–0.6 at% for 10 min and 1.4–1.7 at% for 1 h of doping time), the difference in the shape and size of the counterion affects the memristive properties of the doped systems. We have shown that substitution after 10 min is more effective than after 60 min for both $CuCl_2$ and $FeCl_3$. The slope of the *I–V* curve and the opening of the loop are highest for $FeCl_3$ after 10 min. Additionally, the non-linear nature of the *I–V* curves suggests typical Schottky barrier thermionic emission characteristics of the samples.

4. Experimental section

Materials

Triethylamine (TEA, ≥99.5%), 3-(trimethylsilyl)propargyl alcohol (99%), diethyldithiocarbamic acid diethylammonium salt (97%) and bicyclo[2.2.1]hepta-2,5-diene-rhodium(I) chloride dimer (Rh, ≥98%) and chloroform-D (99.8% atom %D) were obtained from Sigma-Aldrich (St. Louis, MO, USA). Tetrahydrofuran (p.a.), toluene (p.a.), methanol (p.a.), dichloromethane (p.a.), ethyl acetate (p.a.), anhydrous magnesium sulfate (p.a.), nitromethane (p.a.), ammonium chloride (p.a.), potassium carbonate (p.a.) were obtained from Chempur (Piekary Slaskie, Poland). Methacryloyl chloride, (97% contain up to 15% of dimer, stabilized) was obtained from Alfa Aesar (Ward Hill, MA, USA). 4-(chloromethyl)phenyltriethoxysilane was obtained from

Fluorochem (Hadfield, United Kingdom). Diethyl ether (99.5%, BHT stabilized), ethyl alcohol (99.8%, p.a.) (was further dehydrated on molecular sieves 4 Å beads, 8–12 mesh from Sigma-Aldrich) and ammonia solution (25%, p.a.) were obtained from POCH (Gliwice, Poland). Iron(III) chloride (98%, anhydrous) was obtained from Thermo Scientific Chemicals (Waltham, Massachusetts, USA). Hydrogen peroxide solution (30%, p.a.) was obtained from Millipore Sigma (Burlington, MA, USA). ITO conductive glass (thickness 1.1 mm, resistance 10 Ω) were obtained from BTC (Legionowo, Poland).

Synthesis of 3-trimethylsiliylpropagyl methacrylate (TPM)

3-Trimethylsiliylpropagyl methacrylate monomer (TPM) was obtained using the synthesis described by Ishizone[57] with some modifications. A solution of 0.92 ml, 9.4 mmol of freshly distilled methacroyl chloride in 15 ml anhydrous diethyl ether was added dropwise to a solution of 3-trimethylsililylpropagyl alcohol (1.16 ml, 7.82 mmol) and triethylamine (2.18 ml, 15.6 mmol) in 15 ml of anhydrous diethyl ether cooled to −10 °C in an ice–salt bath. The solution was then left for 1 h in the bath and then for another 4 h at ambient temperature. Then it was washed twice with 20 ml of concentrated aqueous ammonium chloride solution and then twice with water. The product was then extracted from the combined water phases by washing them with 20 ml of ethyl acetate. The organic phases were combined, dried with anhydrous magnesium sulfate, condensed on a rotary evaporator, and purified by distillation (boiling point 71 °C under 10 mbar). The reaction was confirmed by infrared and nuclear magnetic resonance spectroscopy (see Fig. S1–S3).

Synthesis of poly(3-trimethylsiliylpropagyl methacrylate) brushes (poly(TPM))

The ITO coated glass substrates were cleaned by sonication in methanol for 20 min and then using a basic piranha solution (1 : 1 concentrated ammonia and 30% hydrogen peroxide at 65 °C), washed with water, acetone, and dried. The substrates were then decorated with 10 ml of 1% 4-(chloromethyl)phenyltriethoxysilane solution in toluene under argon gas for 24 h (see Fig. 4a). They were later cleaned by sonication for 10 min in toluene and 5 min for water, washed with water and acetone, and dried. Surface photoinfiter was obtained by treating decorated substrates with a solution containing 5.5 mg of diethyldithiocarbamic acid diethylammonium salt in 5 ml of tetrahydrofuran (THF) for 24 h under argon. Polymerization was carried out using a deoxygenated solution containing 40 μl of monomer and 360 μl of absolute ethanol and LED with 275 nm maximum of emission for 8 h. Obtained brushes (see Fig. 4b) were cleaned by washing with THF, and characterized with grazing angle infrared spectroscopy and atomic force microscopy.

Self-templating polymerization and doping of poly(3-trimethylsiliylpropagyl methacrylate) brushes

The propagyl side groups in brushes were cleaved by treating them with a concentrated solution of potassium carbonate solution in a 1 : 1 vol methanol/THF mixture under argon for 1 h (see Fig. 4c), washed with acetone and dried. Template polymerization was carried out in a solution containing 5 mg of Bicyclo[2.2.1]hepta-2,5-diene-rhodium(I) chloride dimer, 3 μl mg of TEA in 10 ml of dichloromethane under argon for 24 h (see Fig. 4d). The obtained conjugated poly(TPM) brushes were then subjected to the doping process, in which two different structures were obtained: one doped with $FeCl_3$ and the other with $CuCl_2$. The doping process was performed using a solution of 20 mg of anhydrous ferric chloride or copper chloride in 2 ml of nitromethane. All reactions were performed under an inert argon atmosphere. To study the influence of doping time on the structure and properties of the obtained structures, doping reactions for each dopant were carried out for 10 and 60 min. Finally, systems of polymer brushes with various degrees of substitution of the appropriate counterions were obtained: $[FeCl_4]^-$ (see Fig. 4e) and $[CuCl_2]^-$ (see Fig. 4f).

Methods

NMR ^1H and ^{13}C spectra were recorded on a Bruker Avance III 400 MHz spectrometer in deuterated chloroform. Chemical shifts are reported in ppm relative to the trimethylsilyl group present in the measured compound and visualized using MestReNova 6.0 (Mestrelab, Santiago de Compostela, Spain).

FTIR spectra were recorded using the Nicolet iS10 spectrometer (Thermo Fisher, Waltham, MA, USA). The spectrum of monomer was obtained using attenuated total reflectance (ATR) while the spectra of brushes grafted on ITO-coated glass substrates were obtained with a grazing angle reflectance accessory (GA-FTIR) at 80°. P-polarized radiation was used and the results were averaged over 128 measurements. Bare ITO substrates used as measurement backgrounds were cleaned using the same procedure as ITO for brush synthesis (see 2.3). The baselines were corrected using dedicated OMNIC 9.2 software (Thermo Fisher). Atomic force microscope (AFM) images were obtained with Dimension Icon XR microscope (Bruker, Santa Barbara, CA, USA) working in the air in the PeakForce Tapping (PFT) mode, using standard silicon cantilevers with a nominal spring constant of 0.4 N m^{-1}, triangular geometry tip and nominal tip radius of 2 nm. All measurement parameters (setpoint, lift height and amplitude) have been selected so as not to modify the structure of soft polymer brushes through unwanted excessive compression and structure deformation. AFM data analysis was performed using NanoScope Analysis 1.9 software (Bruker), a dedicated programme for scanning probe microscopy data visualisation and analysis. If necessary, plane fit and flatten functions were used to level the surface of the collected images.

Surface-grafted photoiniferter mediated polymerization (SI-PIMP) was carried out with UV IL-02 irradiating system with a 275 nm monochromatic lamp composed of 112 diodes (ZEiA CHIP, Stalowa Wola, Poland, P_{max}: 150 W, U_{led}: 30–50 V, $I_{led.max}$: 3.5 A) using a 50 W power setting. The reaction was carried out in a system consisting of an iniferter grafted substrate placed inside a UV quartz glass cuvette with a 2 mm path length (Ossila, Sheffield, UK) positioned vertically inside a quartz beaker (Hornik, Quartz, 50 ml, transmittance range:

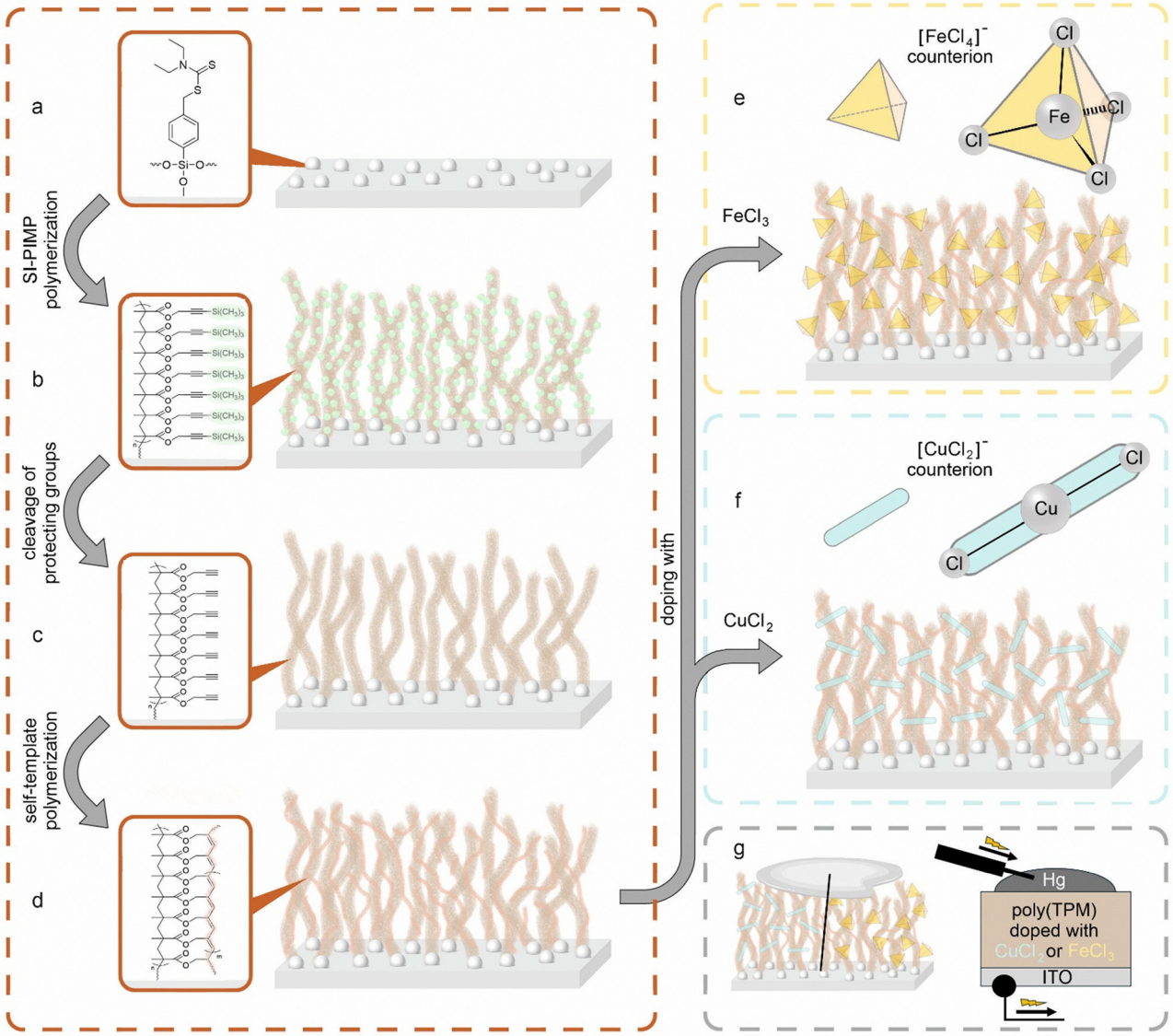

Fig. 4 Scheme of synthesis of poly(TPM) brushes grafted form ITO surface: photoiniferter deposition (a), photoiniferter-mediated polymerization (PIMP) of TPM (b), cleavage of protecting TMS groups (c), self-template polymerization forming polyacetylene conjugated chains (d); poly(TPM) brushes structure doped with $FeCl_3$ (e) and $CuCl_2$ (f); schematic drawing of electrical measurements of poly(TPM) brushes covered with Hg drop as an electrode (g).

160–3500 nm) sealed with a septum positioned 120 mm from the lamp. The monomer solution was transferred *via* a needle to the cuvette after 10 minutes of deoxygenation.

The current–voltage measurements were conducted on SP-150 potentiostat (BioLogic, Seyssinet-Pariset, France) in the −500 to +500 mV voltage window. *I–V* cycles were measured with a scan rate of 200 mV s^{-1} in a series of 10 scans for each sample. Data were collected with the EC-Lab software (v 11.33) then averaged and visualized in OriginPro 2024. Additional scan series with lower voltage scan ranges are presented in the SI. The measurements were performed in the CE to ground mode in 2-terminal configuration. To avoid collapsing of the poly(TPM) brushes the working electrode was composed of a mercury drop connected with the golden wire (Fig. 4g). The reproducibility of the electrode surface was ensured by measuring the same volume of mercury with the pipette each time. After every scan series, the working electrode was replaced to avoid possible contamination.

The Kelvin probe (KP) measurements were performed in the air using a commercial probe (KP01, KP Technology, UK). The WF measurements for all substrates were conducted under ambient conditions within a Faraday cage to minimize external interference. Before each measurement, the samples were allowed to equilibrate with ambient conditions for a minimum of 30 min. For each sample, the number of averaged readings was set to 1000 to ensure accuracy and reproducibility.

The XPS analyses were carried out in a PHI VersaProbe II Scanning XPS system using monochromatic Al Kα (1486.6 eV) X-rays focused to a 100 μm spot and scanned over an area of 400 μm × 400 μm. The photoelectron take-off angle was 45° and the pass energy in the analyzer was set to 117.50 eV (0.5 eV step) for survey scans and 46.95 eV (0.1 eV step) for high energy

resolution spectra. A dual beam charge compensation with 7 eV Ar^+ ions and 1 eV electrons was used to maintain a constant sample surface potential regardless of the sample conductivity. All XPS spectra were charge referenced to the non-functionalized, saturated carbon (C–C) C 1s peak at 285.0 eV. The operating pressure in the analytical chamber was less than 3×10^{-9} mbar. The deconvolution of spectra was carried out using PHI MultiPak software (v.9.9.3). The spectrum background was subtracted using the Shirley method.

Author contributions

M. S. and K. Sz. conceived and planned this research. W. W., T. K., T. M., K. So and M. S. did the experiments. K. Sz. contributed to the DFT simulations. W. W., T. M. and M. S. organized the data. W. W., T. K. and M. S. wrote the manuscript. T. M. and M. S. reviewed the manuscript. M. S. supervised the research and writing of the manuscript. All authors discussed the results and approved the final version of the manuscript.

Conflicts of interest

There are no conflicts to declare.

Data availability

All raw source data of this study (unmodified AFM images, FTIR and XPS spectra, KP data, all *I–V* curves of all charts) and DFT simulation data are available in the Figshare repository – **https://doi.org/10.6084/m9.figshare.28172786**.

Characterization of 3-trimethylsiliylpropagyl methacrylate monomer (TPM) (FTIR, H-NMR, C-NMR spectra), AFM images of poly(TPM) brushes after different PIMP reaction times, XPS survey spectrum for poly(TPM) brushes after self-template polymerization doped with $FeCl_3$ and $CuCl_2$, DFT simulation of spatial conformation of $Fe[Cl_4]^-$ and $Cu[Cl_2]^-$ counterions, *I–V* plots characteristic for various voltage ranges (−200 mV to +200 mV, −300 mV to +300 mV, −400 mV to +400 mV). See DOI: **https://doi.org/10.1039/d5tc01634g**

Acknowledgements

This study was funded by National Science Centre (Poland) [Sonata Bis Grant no. 2021/42/E/ST4/00290]. The research project was also partly supported by program ''Excellence Initiative – Research University'' for the AGH University of Krakow. The funders played no role in study design, data collection, analysis and interpretation of data, or the writing of this manuscript.

References

1 Y. Xiao, B. Jiang, Z. Zhang, S. Ke, Y. Jin, X. Wen and C. Ye, *Sci. Technol. Adv. Mater.*, 2023, **24**, 2162323.
2 M. Zolfagharinejad, U. Alegre-Ibarra, T. Chen, S. Kinge and W. G. van der Wiel, *Eur. Phys. J. B*, 2024, **97**, 70.
3 N. Margalit, C. Xiang, S. M. Bowers, A. Bjorlin, R. Blum and J. E. Bowers, *Appl. Phys. Lett.*, 2021, **118**, 220501.
4 N. K. Upadhyay, H. Jiang, Z. Wang, S. Asapu, Q. Xia and J. Joshua Yang, *Adv. Mater. Technol.*, 2019, **4**, 1800589.
5 L. F. Abbott and W. G. Regehr, *Nature*, 2004, **431**, 796–803.
6 L. Wang, C. Yang, J. Wen, S. Gai and Y. Peng, *J. Mater. Sci.: Mater. Electron.*, 2015, **26**, 4618–4628.
7 L. Chua, *IEEE Trans. Circuit Theory*, 1971, **18**, 507–519.
8 D. B. Strukov, G. S. Snider, D. R. Stewart and R. S. Williams, *Nature*, 2008, **453**, 80–83.
9 S. P. Adhikari, M. P. Sah, H. Kim and L. O. Chua, *IEEE Trans. Circuits Syst. I: Regul. Pap.*, 2013, **60**, 3008–3021.
10 S. Saïghi, C. G. Mayr, T. Serrano-Gotarredona, H. Schmidt, G. Lecerf, J. Tomas, J. Crollier, S. Boyn, A. F. Vincent, D. Querlioz, S. La Barbera, F. Alibart, D. Buillaume, O. Bichler, C. Gamrat and B. Linares-Barranco, *Front. Neurosci.*, 2015, **9**, 51.
11 A. Chanthbouala, V. Garcia, R. O. Cherifi, K. Bouzehouane, S. Fusil, X. Moya, S. Xavier, H. Yamada, C. Deranlot, N. D. Mathur, M. Bibes, A. Barthelemy and J. Grollier, *Nat. Mater.*, 2012, **11**, 860–864.
12 M. L. Wu, C. P. Yang, D.-W. Shi, R. L. Wang, L. F. Xu, H.-B. Xiao and K. Baerner, *AIP Adv.*, 2014, **4**, 047123.
13 Y. Yilmaz and P. Mazumder, *IEEE Trans. Very Large Scale Integr. VLSI Syst.*, 2013, **21**, 1181–1188.
14 T. Kawahara, K. Ito, R. Takemura and H. Ohno, *Microelectron. Reliab.*, 2012, **52**, 613–627.
15 G. Zhou, Z. Ren, L. Wang, B. Sun, S. Duan and Q. Song, *Mater. Horiz.*, 2019, **6**, 1877–1882.
16 W.-S. Nam, S.-H. Seo and J.-G. Park, *Electrochem. Solid-State Lett.*, 2011, **14**, H277.
17 Y. Yin, Z. Liu, M. Song, S. Ju, X. Wang, Z. Zhou, H. Mao, Y. Ding, J. Liu and W. Huang, *J. Mater. Chem. C*, 2018, **6**, 11162–11169.
18 Y.-K. Fang, C.-L. Liu and W.-C. Chen, *J. Mater. Chem.*, 2011, **21**, 4778.
19 Y. Lai, Y.-X. Wang, Y.-C. Huang, T.-Y. Lin, Y.-P. Hsieh, Y.-J. Yang and Y.-F. Chen, *Adv. Funct. Mater.*, 2014, **24**, 1430–1438.
20 Y. Cao, B. Zhang, X. Tian, M. Gu and Y. Chen, *Nanoscale*, 2019, **11**, 3527–3533.
21 G. Natta, G. Mazzant and P. Corradini, *Rend. Lincei. Sci. Fis. Nat.*, 1958, **25**, 3–12.
22 S. Wang, Q. Sun, O. Groning, R. Widmer, C. A. Pignedoli, L. Cai, X. Yu, B. Yuan, C. Li, H. Ju, J. Zhu, P. Ruffieux, R. Fasel and W. Xu, *Nat. Chem.*, 2019, **11**, 924–930.
23 H. Shirakawa, E. J. Louis, A. G. MacDiarmid, C. K. Chiang and A. J. Heeger, *J. Chem. Soc., Chem. Commun.*, 1977, **16**, 578.
24 T. C. Clarke, B. W. Mcquillan, J. F. Rabolt, J. C. Scott and G. B. Street, *Mol. Cryst. Liq. Cryst.*, 1982, **83**, 1–16.
25 A. J. Dianoux, G. R. Kneller, J. L. Sauvajol and J. C. Smith, *J. Chem. Phys.*, 1994, **101**, 634–644.
26 H. Goto, *IOP Conf. Ser. Mater. Sci. Eng.*, 2014, **54**, 012019.

27 Y. W. Park, W. K. Han, C. H. Choi and H. Shirakawa, *Phys. Rev. B: Condens. Matter Mater. Phys.*, 1984, **30**, 5847–5851.
28 H. Kuroda, I. Ikemoto, K. Asakura, H. Ishii, H. Shirakawa, T. Kobayashi, H. Oyanagi and T. Matsushita, *Solid State Commun.*, 1983, **46**, 235–238.
29 X. Guo, M. Baumgarten and K. Müllen, *Prog. Polym. Sci.*, 2013, **38**, 1832–1908.
30 M. Szuwarzyński, K. Wolski, T. Kruk and S. Zapotoczny, *Prog. Polym. Sci.*, 2021, **121**, 101433.
31 J. Yee Low, Z. M. A. Merican and M. F. Hamza, *Mater. Today Proc.*, 2019, **16**, 1909–1918.
32 C. Di, G. Yu, Y. Liu and D. Zhu, *J. Phys. Chem. B*, 2007, **111**, 14083–14096.
33 C. Dai and B. Liu, *Energy Environ. Sci.*, 2020, **13**, 24–52.
34 Y. Chen, G. Liu, C. Wang, W. Zhang, R.-W. Li and L. Wang, *Mater. Horiz.*, 2014, **1**, 489.
35 M. Szuwarzyński, J. Kowal and S. Zapotoczny, *J. Mater. Chem.*, 2012, **22**, 20179–20181.
36 M. Szuwarzyński, K. Wolski and S. Zapotoczny, *Polym. Chem.*, 2015, **7**, 5664–5670.
37 W. J. Brittain and S. Minko, *J. Polym. Sci. A. Polym. Chem.*, 2007, **45**, 3505–3512.
38 N. Kang, B. Cho, B. Kang, S. Song, T. Lee and J. Lee, *Adv. Mater.*, 2012, **24**, 385–390.
39 K. Wolski, M. Szuwarzyński, M. Kopeć and S. Zapotoczny, *Eur. Polym. J.*, 2015, **65**, 155–170.
40 K. Wolski, M. Szuwarzyński and S. Zapotoczny, *Chem. Sci.*, 2015, **6**, 1754–1760.
41 R. M. Hensarling, V. A. Doughty, J. W. Chan and D. L. Patton, *J. Am. Chem. Soc.*, 2009, **131**, 14673–14675.
42 M. Szuwarzyński, K. Wolski, A. Pomorska, T. Uchacz, A. Gut, Ł. Łapok and S. Zapotoczny, *Chem. – Eur. J.*, 2017, **23**, 11239–11243.
43 R. Huq and G. C. Farrington, *J. Electrochem. Soc.*, 1984, **131**, 819–823.
44 A. Kumar, S. Pandey, P. Tandon and V. D. Gupta, *J. Macromol. Sci.*, 2000, **39**, 303.
45 A. D. Wagner, A. V. Naumkin, A. Kraut-Vass, J. W. Allison, C. J. Powell and J. R. J. Rumble, *NIST Standard Reference Database, SRD 20*, National Institute of Standards and Technology, USA, 2003.
46 M. Fantauzzi, B. Elsener, D. Atzei, A. Rigoldi and A. Rossi, *RSC Adv.*, 2015, **5**, 75953–75963.
47 G. Beamson and D. Briggs, *J. Chem. Educ.*, 1993, **70**, A25.
48 M. J. Genet, C. C. Dupont-Gillain and P. G. Rouxhet, *Medical Applictions of Colloids*, Springer Science Business Media, LLC, 2008.
49 C. D. Wagner, D. E. Passoja, H. F. Hillery, T. G. Kinisky, H. A. Six, W. T. Jansen and J. A. Taylor, *J. Vac. Sci. Technol.*, 1982, **21**, 933–944.
50 J. Salgado-Beceiro, J. M. Bermúdez-García, A. L. Llamas-Saiz, S. Castro-García, M. A. Señarís-Rodríguez, F. Rivadulla and M. Sánchez-Andújar, *J. Mater. Chem. C*, 2020, **8**, 12686.
51 R. Peng, M. Li and D. Li, *Coord. Chem. Rev.*, 2010, **254** 1–18.
52 T. Mazur, P. Zawal and K. Szaciłowski, *Nanoscale*, 2019, **11**, 1080–1090.
53 K. Berke, S. Tongay, M. McCarthy, A. Rinzler, B. Appleton and A. Hebard, *J. Condens. Matter. Phys.*, 2012, **24**, 255802.
54 I. Valov, *Semicond. Sci. Technol.*, 2017, **32**, 093006.
55 S. Kim, S. Choi, J. Lee and W. D. Lu, *ACS Nano*, 2014, **8**, 10262–10269.
56 Y. Zhu, K. Xue, X. Cheng, C. Qiao, J. Yuan, L. Li and X. Miao, *Appl. Surf. Sci.*, 2021, **550**, 149274.
57 T. Ishizone, G. Uehara, A. Hirao, S. Nakahama and K. Tsuda, *Macromol. Chem. Phys.*, 1998, **199**, 1827–1834.